Cell Reports
Article

Crystal Structure and Mechanism of Activation of TANK-Binding Kinase 1

Amede Larabi,[1] Juliette M. Devos,[1] Sze-Ling Ng,[2] Max H. Nanao,[1] Adam Round,[1] Tom Maniatis,[2,3] and Daniel Panne[1,*]
[1]EMBL Grenoble, 6 Rue Jules Horowitz, Grenoble 38042, France
[2]Department of Molecular and Cellular Biology, Harvard University, Cambridge 02138, MA, USA
[3]Present address: Department of Biochemistry and Molecular Biophysics, Columbia University, New York, NY 10032, USA
*Correspondence: panne@embl.fr
http://dx.doi.org/10.1016/j.celrep.2013.01.034

SUMMARY

Tank-binding kinase I (TBK1) plays a key role in the innate immune system by integrating signals from pattern-recognition receptors. Here, we report the X-ray crystal structures of inhibitor-bound inactive and active TBK1 determined to 2.6 Å and 4.0 Å resolution, respectively. The structures reveal a compact dimer made up of trimodular subunits containing an N-terminal kinase domain (KD), a ubiquitin-like domain (ULD), and an α-helical scaffold dimerization domain (SDD). Activation rearranges the KD into an active conformation while maintaining the overall dimer conformation. Low-resolution SAXS studies reveal that the missing C-terminal domain (CTD) extends away from the main body of the kinase dimer. Mutants that interfere with TBK1 dimerization show significantly reduced *trans*-autophosphorylation but retain the ability to bind adaptor proteins through the CTD. Our results provide detailed insights into the architecture of TBK1 and the molecular mechanism of activation.

INTRODUCTION

Inhibitor of κB kinases (IKKs) are essential regulators of the inflammatory, immune, and apoptotic responses. Canonical IKK signaling is mediated by the multicomponent IKK complex, which is composed of two kinase subunits, IKKα and IKKβ, and the regulatory scaffold subunit NEMO (nuclear factor κB [NFκB] essential modifier; also called IKKγ) (Chen et al., 1996; DiDonato et al., 1997; Mercurio et al., 1997; Zandi et al., 1997). The canonical IKKs activate the transcription factor NFκB by phosphorylating the inhibitor of κB proteins. This phosphorylation leads to the ubiquitination and proteasome-dependent degradation of IκB. In addition to IKKα and IKKβ, the IKK kinase family contains two noncanonical family members IKKε and TBK1 (Peters and Maniatis, 2001; Pomerantz and Baltimore, 1999; Shimada et al., 1999). Although these two kinases have similar biochemical properties in vitro, they have very different functions in vivo (Ng et al., 2011; Tenoever et al., 2007). TBK1 is activated by pattern-recognition receptors, such as Toll-like receptors, and intracellular receptors, such as RIG-I, MDA5, or DAI, and it phosphorylates IRF3 and IRF7 and other target proteins (Clément et al., 2008). TBK1 is essential for the activation of type I interferon (IFN) in vivo, while IKKε is not. In fact, IKKε is required for the activation of IFN-stimulated genes in vivo and is not required for IFN expression. IKKε functions by phosphorylating a specific serine residue in the transcription factor STAT1, and thereby controlling the assembly of IFN-inducible transcription factor complexes (Ng et al., 2011; Tenoever et al., 2007). The activation loop of TBK1 and IKKε contains only a single phosphoacceptor site (S172) in the T-loop but the mechanisms by which these kinases are activated are not understood. The canonical and noncanonical IKK kinases share ~28% sequence identity and a similar domain organization with an N-terminal kinase domain (KD) followed by a ubiquitin-like domain (ULD), a helical scaffold dimerization domain (SDD) and a C-terminal domain (CTD) (Figure 1A) (Xu et al., 2011). The crystal structure of *Xenopus* IKKβ (xIKKβ) showed that the KD and ULD associate with the SDD indicating that the three modules operate as a trimodular unit. The xIKKβ structure also showed that dimerization is mediated by a C-terminal region of the SDD (Xu et al., 2011).

IKKs interact with scaffold proteins that are required for their activation. Canonical IKKs interact with NEMO: the noncanonical TBK1 and IKKε with the adaptor proteins TANK (TRAF family member associated NFκB activator), NAP1 (NAK-associated protein 1), SINTBAD (similar to NAP1 TBK1 adaptor), or optineurin (Fujita et al., 2003; Gatot et al., 2007; Guo and Cheng, 2007; Morton et al., 2008; Ryzhakov and Randow, 2007). These adaptors are predicted to be structurally similar to NEMO, which forms an elongated parallel dimeric coiled coil (Israël, 2010). NEMO contains an ubiquitin-binding domain and binds linear or K63-linked polyubiquitin chains (Baker and Ghosh, 2009). IKK activation depends on NEMO, and ubiquitination may allow recruitment of an activating kinase such as TAK1 or may trigger IKK oligomerization, leading to *trans*-autophosphorylation in the T-loop and activation of the kinase subunits (Baker and Ghosh, 2009). An important question is how IKK kinases are activated and the role of ubiquitin signaling in that process.

NFκB signaling pathways are implicated in numerous human diseases (Karin et al., 2004). Recent findings point toward a

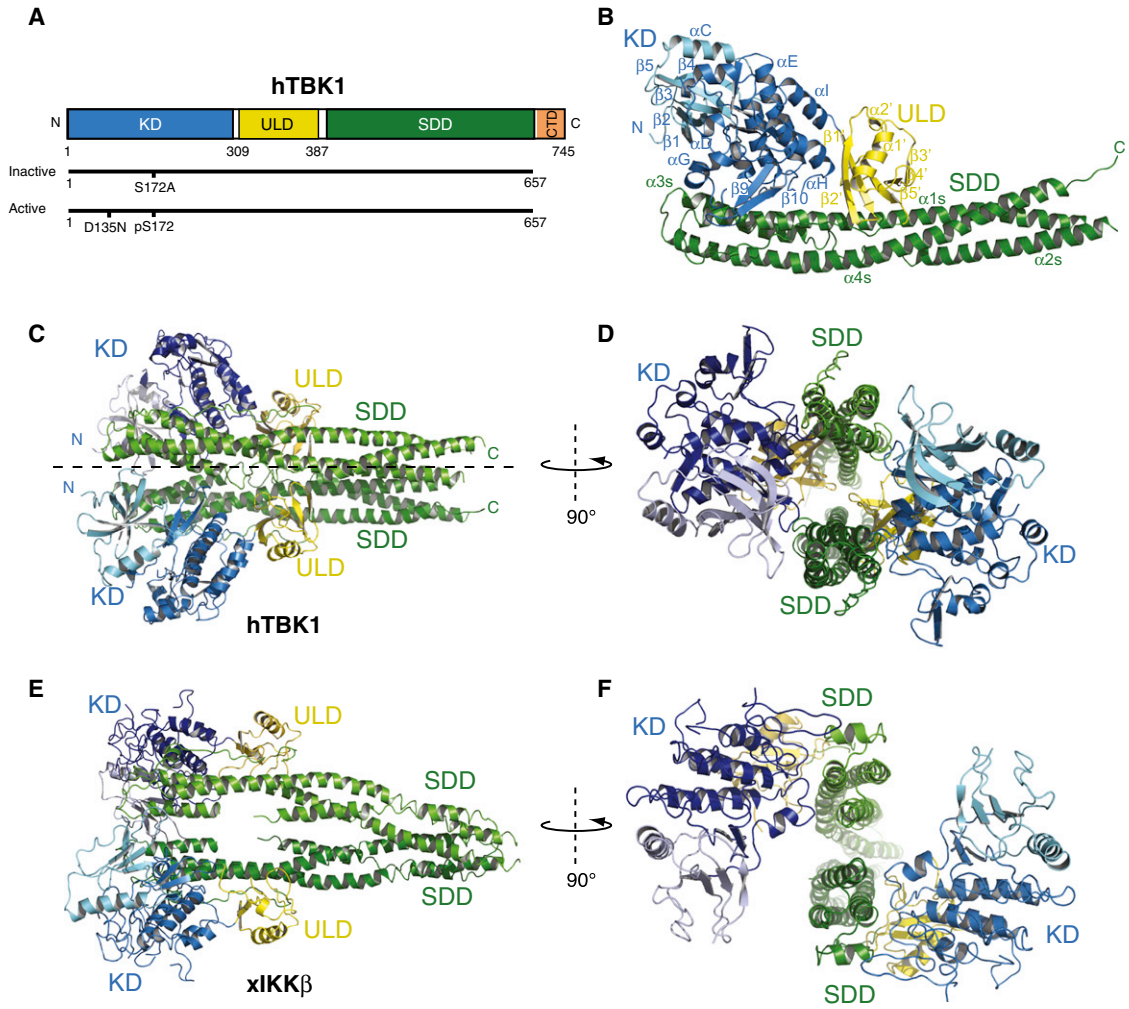

Figure 1. Structure of hTBK1

(A) Cartoon showing domain boundaries for the KD, ULD, SDD, and CTD. The crystallized constructs are shown below. Inactive TBK1 was crystallized using a construct containing a S172A mutation. Active TBK1 was crystallized using a S172-phosphorylated construct containing a D135N mutation.

(B) The KD, ULD, and SDD are shown in blue, yellow, and green, respectively. Secondary structure elements are labeled, with those in the ULD indicated with a prime and those in the SDD by an "s".

(C) Structure of the hTBK1 dimer. The 2-fold symmetry axis is indicated by a dashed line.

(D) View along the 2-fold symmetry axis of TBK1.

(E and F) Structure of the xIKKβ dimer for comparison.

See also Figures S1D and S1E.

role of TBK1 and IKKε in oncogenic transformation. In addition to its role in inflammatory pain and obesity, IKKε has been shown to be upregulated in breast, ovarian and prostate cancer cell lines and in patient-derived tumors (Adli and Baldwin, 2006; Boehm et al., 2007; Guo et al., 2009; Möser et al., 2011; Olefsky, 2009; Péant et al., 2009). TBK1 has been shown to be involved in Ras-induced cell transformation (Barbie et al., 2009; Chien et al., 2006; Xie et al., 2011). Recent work has identified the survival signaling kinase AKT as a direct substrate of TBK1 (Ou et al., 2011). As a result, TBK1 and IKKε have drawn considerable attention and have become novel drug targets with applications in the treatment of cancer and a variety of inflammatory diseases including rheumatoid arthritis and obesity-related metabolic disorders. The structures of these kinases are therefore of considerable interest.

RESULTS

Crystal Structure of Inactive TBK1

We obtained crystals of a C-terminally truncated kinase fragment (residues 1–657; Figure 1A) and determined the structure in complex with specific TBK1 inhibitors (BX795 (Clark et al., 2009, 2011), MRT67307 and MRT67215) to a resolution of 2.6 Å using anomalous diffraction methods with selenomethionine-derivatized protein (Table S1). The construct contained a S172A mutation that inactivates the enzyme and allowed

purification of unphosphorylated TBK1 (Figures S1A and S1B). The entire polypeptide is well ordered, except for residues 166–174 and 187–198 of the activation loop and residues 483–492 in the SDD, which were not modeled.

The crystals of inactive TBK1 are in space group $P3_221$ and contain a single copy in the asymmetric unit. Figure 1B shows a side view of the structure with a N-terminal KD (residues 1–307), the ULD (309–384), and the all-helical SDD (408–654). Both full-length and C-terminally truncated TBK1 are dimers in solution (see below). A crystallographic 2-fold axis runs along the long axis of the molecule and generates the TBK1 dimer (Figure 1C). The dimensions of the dimer are ~110 × 133 × 80 Å and the overall trimodular architecture resembles that of the previously determined IKKβ structure (Figure 1E; Xu et al., 2011). However, there are major differences between the two structures. As compared to TBK1, the KD of IKKβ rotates by ~45°, and its center of mass translates ~8 Å away from the dimer axis (Figure 1E). The ULD of IKKβ rotates by ~30° and shifts ~10 Å away from the dimer axis, while maintaining the attachment to the SDD. As a result, the overall organization of the kinase dimers is different: the TBK1 dimer is compact and dimerization is mediated by several interfaces involving the KD, the ULD and SDD, distributed along the entire length of the molecule (Figure 1C). The IKKβ dimer is in a more "open" conformation and there are few interactions along the long axis of the molecule. A small interface in the C terminus of the SDD mediates IKKβ dimerization (Figure 1E). A view along the 2-fold axis of the dimer shows that the KDs of IKKβ have rotated apart (compare Figures 1D and 1F).

Crystal Structure of Active TBK1

The fact that the crystallized IKKβ construct contains two mutations (S177E/S181E) that render the kinase constitutively active and the TBK1 construct an inactivating mutation (S172A) suggested that dimer rearrangement might be part of the activation mechanism of IKK kinases. To test this model, we determined the 4.0 Å resolution crystal structure of active, S172-phosphorylated TBK1 containing residues 1–657 (Table S1). We obtained these crystals from a construct containing a catalytic residue mutation D135N (Figure 1A). This construct was monophosphorylated on S172 using wild-type TBK1 and crystallized in the presence of the inhibitor BX795. The crystals of active TBK1 are in space group $P6_522$ and contain a single copy in the asymmetric unit. The entire polypeptide including the activation loop is well ordered, except for residues 485– 492 in the SDD (Figure S1D).

We find that the structure of active and inactive TBK1 superimpose with an rmsd of ~1.5 Å (for 603 Cα residues) and that the dimerization interface is maintained (Figure S1E). However, the structures of the active and inactive KDs are significantly different (Figure 2): the conformation of the inactive KD is similar to that seen in the crystal structures of other inactive kinases such as CDK2 or Src (De Bondt et al., 1993; Xu et al., 1997). Helix αC (residues 50–62) in the catalytic domain of TBK1 is swung outward relative to its position in the active conformation (Figure 2A). As a result of this displacement, conserved E55 is rotated away from the active site, and the so-called "regulatory spine," assembly of which is required in active kinases, is disrupted (Kornev and Taylor, 2010). The structure of TBK1 displays another feature characteristic of an inactive kinase conformation, which is the formation of a short 3_{10} helix (residues 160–164) at the beginning of the activation loop, immediately following the conserved DFG motif (residues 157–159). This short helix packs against the outwardly displaced helix αC and helps to stabilize its displacement. The remainder of the activation loop, except for a stretch containing parts of helix αEF (residues 175–186), is disordered. In contrast, in the active, S172-phosphorylated form, the activation loop is fully ordered. The phosphoserine makes contacts to R54 in the C helix, R134 in the catalytic loop and R162 in the activation loop (Figure 2B). L164 shifts by 15 Å from its position in the inactive conformation, resulting in remodeling of the autoinhibitory 3_{10} helix. This allows a ~57° rotation of the C helix toward the active site. In this conformation, E55 makes a salt bridge with K38 in β5. Reorganization of the activation loop yields a conformation that is suitable for substrate binding. Superposition with the protein kinase A (PKA) peptide inhibitor (PKI) complex based on alignment of the KDs suggests that TBK1 would also favor a hydrophobic residue at the P+1 position of the substrate (Figure S2E; Ma et al., 2012).

Structural comparison of kinase structures shows that activation frequently requires rotation of the N-lobe relative to the C-lobe of the KD (Lei et al., 2005; Steichen et al., 2012). Comparison of the active and inactive conformations of TBK1 shows no such structural transitions. Although activation of TBK1 does require reorganization of the activation loop and the C helix, this does not require repositioning of the N-lobe, and, as a result, dimerization contacts involving N- and C-lobe of the kinase are maintained (see below). The structure of the active KD superimposes with the structure of the isolated KD with an rmsd of 0.8 Å and is similar to that usually seen in structures of active KDs (Ma et al., 2012).

The inhibitors bind in a similar manner to the active and inactive KDs: they are positioned in the cleft between the N- and C-lobes and occupy several subregions of the ATP binding site to bury a surface area of ~450 $Å^2$ (Figures 2C, 2D, and S2A–S2D). The presence of the inhibitor stabilizes the so-called "catalytic spine" of the kinase, which is in an assembled conformation (Kornev and Taylor, 2010). Location of the inhibitors confirms earlier proposals that these compounds are ATP competitive (Clark et al., 2009). All three inhibitors share a common 2,4-bis anilino pyrimidine core structure, which binds in a similar manner to the hinge region of TBK1. Two hydrogen bonds are formed between the backbone nitrogen and carbonyl group of C89 of the kinase hinge with nitrogens in the pyrimidine and aniline moieties (Figure 2C). The pyrimidine ring makes hydrophobic contacts with M142 and A36, whereas the aniline moiety is sandwiched between G92 and L15. The three compounds are derivatized at the aniline and pyrimidine rings. In MRT67307, the cyclopropyl group at the C5 position of the pyrimidine ring makes hydrophobic contacts to A36, T156, and the gatekeeper residue M86. The cyclobutylcarboxamide moiety penetrates deepest into the ATP binding pocket and makes hydrophobic contacts with G18, A21, Val23 and packs against the side chain of D157 of the DFG motif. Its carbonyl group forms a hydrogen bond with the backbone nitrogen of D157. On the other end of the

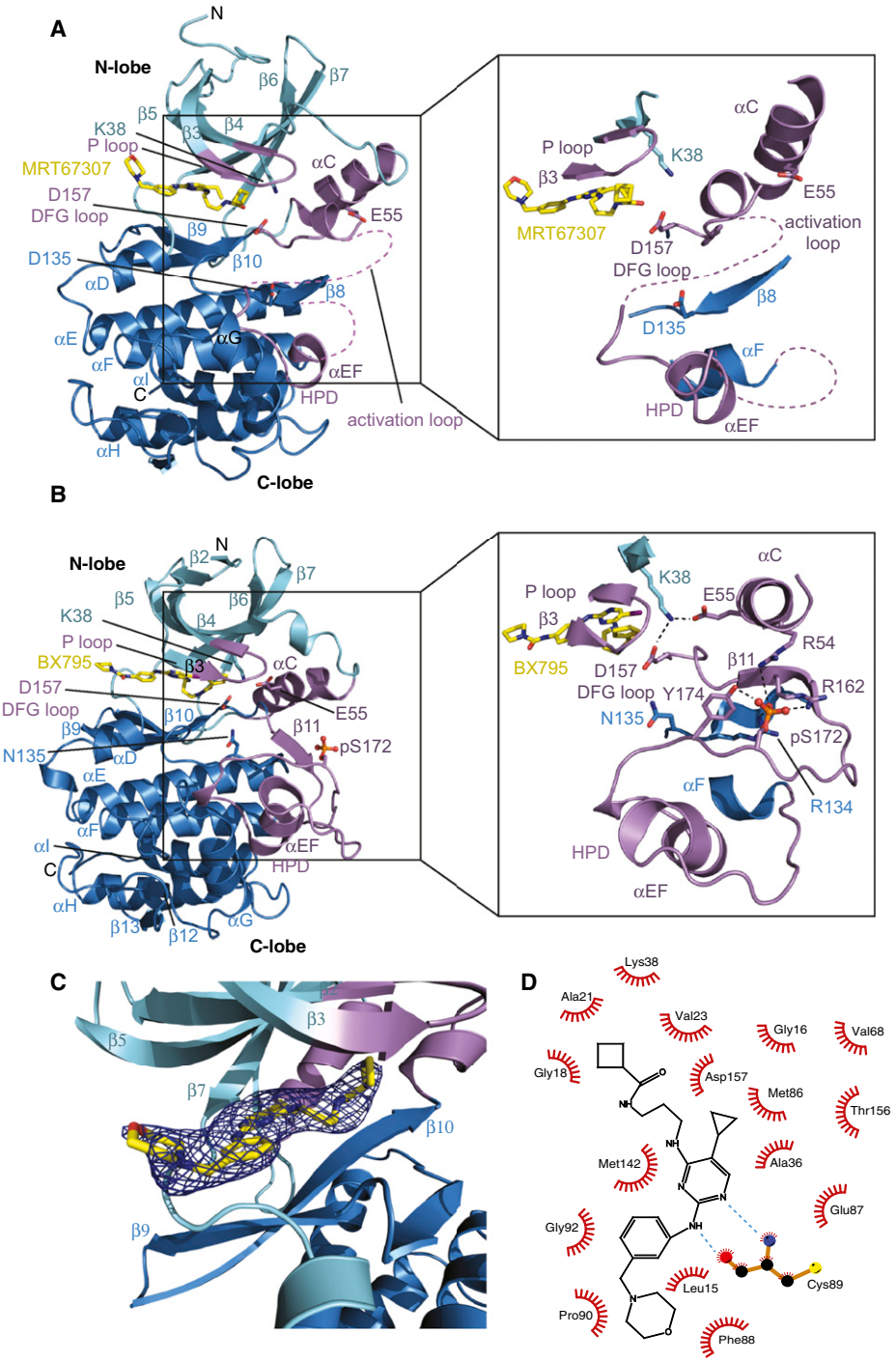

Figure 2. Structure of Inactive and Active KD and Inhibitor Binding

(A) The inactive KD. The N-lobe is shown in light blue, the C-lobe in dark blue and structural elements of the active site in magenta. The inset displays important components of the kinase active site: helix αC, P loop, and the catalytic residues: Asp157 (DFG motif), Asp135 (HRD motif), catalytic lysine Lys38, and glutamate Glu55. The activation loop is disordered and approximate location is shown as a dotted line.

(B) The active KD. The activation loop is ordered in the pS172-phosphorylated form. The inset shows a closeup view of the activation loop with the side chains of pS172, R54, R134, R162, and Y174 shown in stick representation. The C helix rotates by ~57° toward the active site allowing E55 to make a salt bridge with K38. A network of hydrogen bonds (black dashed lines) involving the phosphate group of pS172 stabilizes the conformation of the activation loop.

(C) F_o-F_c electron density omit map for MRT67307 contoured at 2σ.

(D) Interactions of MRT67307 with the KD. Generated with the program LIGPLOT.

See also Figure S2.

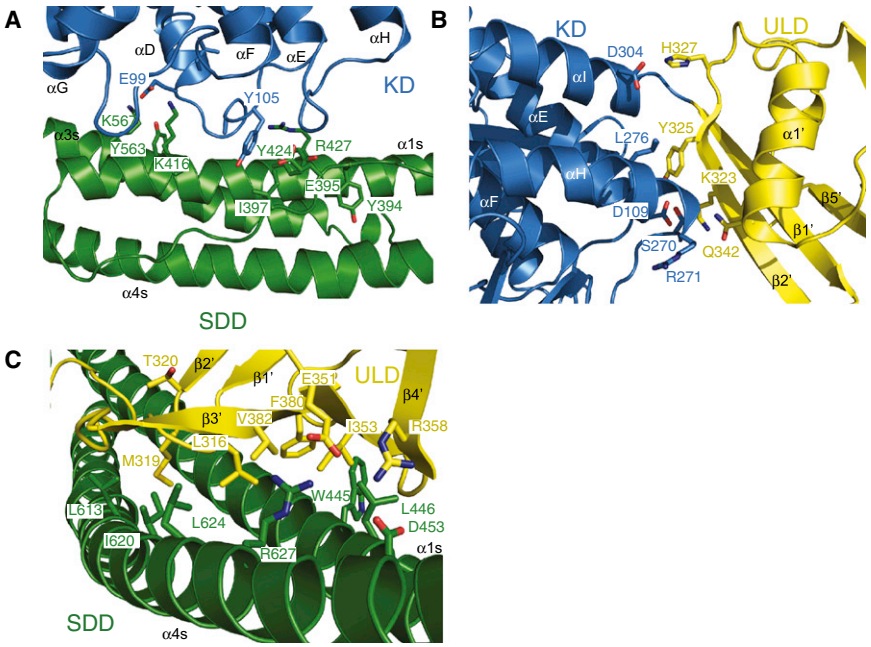

Figure 3. Interactions between the KD, ULD, and SDD

(A) Interaction between KD (blue) and SDD (green). Residues in the interface are shown with nitrogen, oxygen, and sulfur atoms in blue, red, and yellow, respectively. Carbon atoms are colored yellow (ULD) or green (SDD).

(B) Interaction between the KD (blue) and ULD (yellow).

(C) Interaction between the ULD (yellow) and SDD (green).

See also Figure S3.

compound, the morpholine moiety is partially buried by interacting with L15, F88, and P90. MRT67307, MRT67215, and BX795 are relatively specific inhibitors of noncanonical IKK kinases but do not inhibit IKKβ or IKKα (Clark et al., 2009). We note that IKKβ and IKKα have an isoleucine instead of T156 preceding the DFG motif, and this residue is predicted to interfere with binding of the noncanonical IKK inhibitors, which carry a bulky substitution at the C5 position of the pyrimidine ring. This steric interference could explain why these compounds are specific for noncanonical IKKs.

Despite low sequence identity with ubiquitin (17%), the ULD of TBK1 adopts the compact ubiquitin-like fold that superposes with a rmsd of 1.9 Å with ubiquitin (Figure S2F). The ULD is sandwiched between the C-lobe of the KD and the SDD (Figure 1B). The hydrophobic patch of ubiquitin that is usually responsible for binding ubiquitin effectors is conserved in the ULD of TBK1 (Ikeda et al., 2007; Li et al., 2012). This surface patch forms a hydrophobic interface with the SDD. The ULD also contacts the C-lobe of the KD and is involved in dimerization contacts. The SDD contains four long helices α1 s-α4 s that form a left-handed, three helical antiparallel coiled coil, which runs along the entire length of the molecule (Figure 1B). As in IKKβ, the C-lobe of the KD binds to the N-terminal end of the SDD and the ULD binds in the middle of the SDD. The C-terminal half of the SDD forms an extended dimerization interface.

Interactions between the KD, ULD, and SDD

The ULD is sandwiched between the C-lobe of the KD and the SDD and adopts a structure similar to that of the isolated domain in solution (Ikeda et al., 2007; Li et al., 2012). A conserved patch of the ULD forms a hydrophobic interface with helices α1 s and α4 s of the SDD (Figure 3C). This interface is mostly hydrophobic and buries a surface area of 1,195 Å^2 (for detailed description of the interface, see Extended Results). The interface includes the conserved I353. The equivalent residue of ubiquitin (I44) is frequently involved in ubiquitin substrate binding (Hicke et al., 2005): burial against the SDD may explain why no known ubiquitin-binding domain binds the ULD (Ikeda et al., 2007). We probed this interface by introducing a destabilizing charged residue within its hydrophobic core (point mutant L316E) and monitored the impact using am IFN-β-luciferase reporter assay in HEK293 cells. It has been previously reported that TBK1 undergoes *trans*-autophosphorylation and activation upon transfection, which we confirmed in our assay: we observed robust induction of the reporter with TBK1wt and phosphorylation of S172 in the activation loop, which we monitored by using a phosphospecific antibody (Figures 4E and S4) (Fitzgerald et al., 2003). As expected, inactivating mutations K38A and S172A did not induce reporter expression and were not phosphorylated on S172 (Figure S4). Expression of these inactivating kinase mutants results in a dominant-negative effect by competing with and disrupting the activity of endogenous TBK1, which is constitutively expressed in this cell line (Fitzgerald et al., 2003). The L316E mutant exhibited 6-fold lower activity than the wild-type kinase but showed normal S172 phosphorylation (Figures 4E and S4). Therefore, although mutagenesis of the ULD-SDD interface clearly impaired IFN-β reporter induction, it did not affect TBK1 activation.

The ULD is rigidly connected to the C-lobe of the KD by a two residue linker between the β1′ of the ULD and helix αI of the KD. The ULD packs against a hydrophobic patch made up of αH and αI of the C-lobe of the KD. Interaction between the two domains buries 379 Å^2 of surface area (Figure 3B, for detailed descriptions of the interface, see Supplemental Information). ULD residue Y325 is buried in this hydrophobic domain interface and forms a hydrogen bond to residue D109 of αE. Y325 is strictly conserved in noncanonical IKKs, and mutation of this residue to glutamate completely abolished S172 phosphorylation and IFN-β reporter activity (Figures 4E and S4). Not surprisingly, deletion of the ULD also completely abolishes kinase activity (Goncalves et al., 2011; Ikeda et al., 2007). Together, these data indicate that the KD-ULD interface plays an essential role in TBK1 kinase activation in vivo.

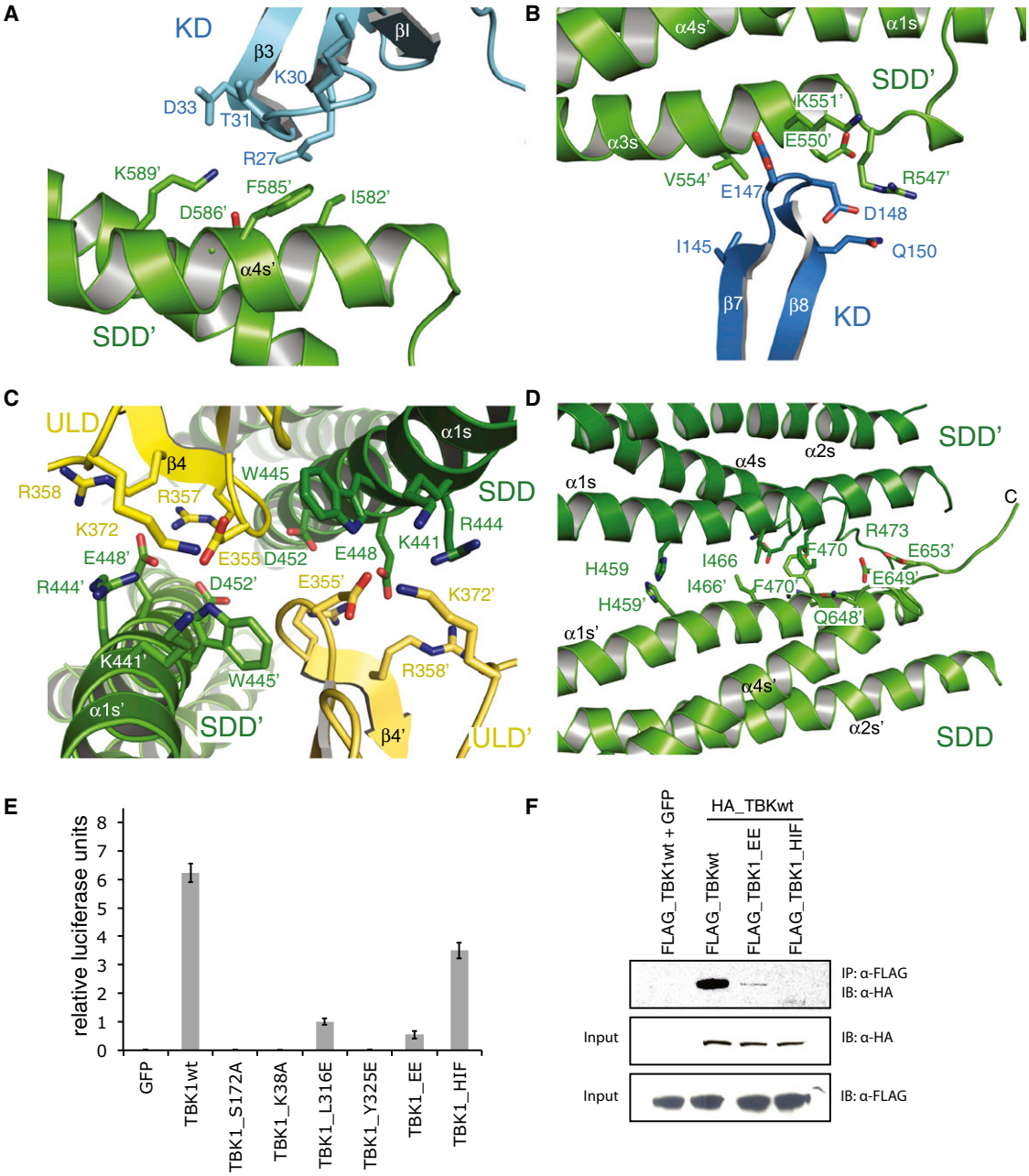

Figure 4. Dimerization Contacts

(A) Interface I: interaction between the N-lobe of the KD (blue) and the SDD′ (green). Residues in the interface are shown with carbon, nitrogen, and oxygen atoms in green, blue, and red, respectively. Secondary structure elements from the second chain are labeled with a prime.

(B) Interface II: interaction between the C-lobe of the KD and SDD′.

(C) Interface III: interaction between the ULD (yellow) and the SDD.

(D) Interface IV: interaction between the two SDDs.

(E) In vivo analysis of TBK1 mutants. 293T cells were transfected with wild-type or mutants. Values represent the mean average of triplicate experiments. Error bars indicate SEM.

(F) 293T cells were transfected with FLAG TBK1wt or mutants and HA TBK1wt. Coimmunoprecipitation (IP) experiments were performed using anti-FLAG matrix beads and immunoblotted (IB) for anti-HA-tagged protein. Input samples were loaded as a control.

See also Figures S3 and S4.

TBK1 Dimerization and Implications in Kinase Regulation

There are four dimerization interfaces that are distributed along the entire length of the molecule: these involve the N-lobe of the KD and the N-terminal end of the SDD (interface I), the C-lobe of the KD and the N-terminal end of the SDD (interface II), the ULD and the central sections of the SDD (interface III), and the C-terminal ends of the SDD (interface IV; Figure 4). Interfaces I and II are small and together bury a total surface area of ~345 Å^2. Interface I includes the β2-β3 loop in the N-lobe of the KD that packs against the N-terminal end of SDD helix α4 s (Figure 4A). Interface II involves the β7-β8 loop of the C-lobe of the kinase that packs against SDD helix α3 s (Figure 4B). Sequence comparison shows that the KD attachment sites on the SDD are conserved among TBK1 and IKKε orthologs and to some degree in IKKα/β (Figure S3). Interface III, which is also conserved among TBK1 orthologs, is mediated by mostly electrostatic interactions involving a loop from the ULD connecting β3′ and β4′ and residues from α1 s of the SDD (Figure 4C). Dimerization buries ~450 Å^2 of surface area. Interface IV is the most extensive, burying ~620 Å^2 surface area on each monomer (Figure 4D). This dimerization interface is mediated by mostly hydrophobic interactions from helix α1 s and helix α4 s (for detailed description of the dimerization contacts, see Extended Results). Taken together, the four dimerization interfaces bury a total surface area of ~1,830 Å^2 per monomer.

One major difference between the TBK1 and IKKβ structures is the dimerization interface. In IKKβ, the dimerization interface is smaller (~1,000 Å^2 of surface area) and is limited to the C-terminal end of the SDD (interface IV) (Xu et al., 2011). Dimerization interfaces I–III are only seen in the TBK1 structure. In TBK1, the KD is anchored at four positions: the C-lobe of the KD forms intramolecular contacts with the SDD and the ULD domain (Figures 3A and 3B). In addition, the N-lobe and the C-lobe of the KD dock against the SDD domain through dimerization interfaces I and II (Figures 4A and 4B). In the IKKβ structure, the KD is only anchored at one position: the C-lobe of the KD is attached to the SDD (Figure 1E). The ULD of IKKβ rotates ~45° away from the C-lobe as compared to its position in TBK1. Therefore, the KD-ULD interface as seen in TBK1 is not present in IKKβ. A view along the 2-fold axis of the dimer shows that the KDs of IKKβ have rotated apart (Figures 1C–1F). As a result, the dimerization contacts mediated by the N- and C-lobe of the KD and ULD (interfaces I–III) are not observed in the IKKβ structure.

To investigate the role of the main dimerization interfaces III and IV for TBK1 function, we generated mutants in each interface and analyzed their impact on the biochemical properties in vitro and functionality in vivo. Two salt bridges between E355 and R444 as well as R357 and D452 stabilize the ULD-SDD interface III. Double mutation of E355R and E448R, which also packs against R357, resulted in lower activity and reduced S172 phosphorylation (Figures 4E and S4). The SDD-SDD interface IV is stabilized by a set of hydrophobic interactions between H459E, I466E, or F470E. Mutation of these residues in combination H459E/I466E/F470E lead to ~2-fold decrease in activity while maintaining autophosphorylation on S172 (Figures 4E and S4). To investigate if dimerization of mutants in vitro correlates with dimerization in vivo, we cotransfected FLAG-tagged TBK1 dimerization mutants with HA-tagged TBK1wt and performed coimmunoprecipitation experiments. Consistent with our in vitro results, we found that all dimerization mutants also abolished dimerization in vivo (Figure 4F).

We purified these mutants and analyzed their biochemical properties in vitro. Full-length TBK1wt and the nonphosphorylated mutant TBK1S172A were dimeric in SEC-MALLS experiments (Figure 5A; Table S2). The crystallization construct was a dimer both in the nonphosphorylated (TBK1S172A_657) and the autophosphorylated (TBK1_657) forms (Figure 5A). In IKKβ, truncation of the C terminus of the SDD leads to monomerization but does not abolish activity (Xu et al., 2011). In TBK1, this region of the protein is part of interface IV. To determine whether this region is required for dimerization, we generated the truncation 1–643 (TBK1_643[S172A]), which removes the part of helix α4 s that is important for IKKβ dimerization. Remarkably, this construct remained dimeric (Figure 5A). Further truncation beyond residue 643 resulted in insolubility of the kinase (data not shown). Thus, in contrast to IKKβ, the C terminus of helix α4 s is dispensable for dimerization mainly because the majority of residues in dimerization interface IV are contributed by helix α1 s. Indeed, mutation of helix α1 s residues H459E/I466E/F470E (TBK1_657_HIF) resulted in monomeric TBK1, showing that interface IV in the SDD is critical for TBK1 dimerization (Figure 5B; Table S2). As dimerization might depend on the phosphorylation status of TBK1, we also produced the nonphosphorylated form TBK_657_HIF(S172A). This mutant protein remained monomeric, showing that this interface IV mutant disrupts dimerization independently of the phosphorylation status (Figure 5B). Residues in interface IV are conserved only among TBK1 orthologs, which likely explains why TBK1 does not heterodimerize with other IKKs (Figure S3). The double mutants E355R/E448R (TBK1_657_EE) in interface III also resulted in monomeric TBK1 (Figure 5B). As expected, the Y325E mutant in the KD-ULD interface (TBK1_657_Y) remained dimeric.

We compared the steady-state kinetic properties of these mutants using an in vitro kinase assay. The apparent K_m value of TBK1_657 for IRF3 was ~80 μM and the apparent V_{max} ~55 μM, whereas the apparent K_m value for ATP was ~78 μM and the apparent V_{max} ~50 μM (Figures 5C and 5D). The TBK1_657_Y mutant showed ~3× reduced activity (Figure 5E). Interface III and IV mutants TBK1_657_HIF and TBK1_657_EE had ~3× and ~6× reduced activity, respectively.

We verified the impact of these mutations on TBK1 activation by monitoring S172 autophosphorylation in the kinase assay. All mutants were already partially autophosphorylated upon overexpression and purification from insect cells as monitored by LC-MS and anti-pS172 immunoblotting (Figures S1A and 5F). The degree of S172 autophosphorylation corresponded well with that seen upon expression in HEK293 cells (Figure S4). Whereas TBK1_657 showed a robust increase in S172 autophosphorylation, the TBK1_657_Y mutant showed reduced autophosphorylation. The dimerization mutants TBK1_657_EE and TBK1_657_HIF also showed weak autophosphorylation. The degree of impairment in autophosphorylation of the mutants corresponded well to the reduced activity as seen in the kinase assay (Figure 5E). We therefore conclude that

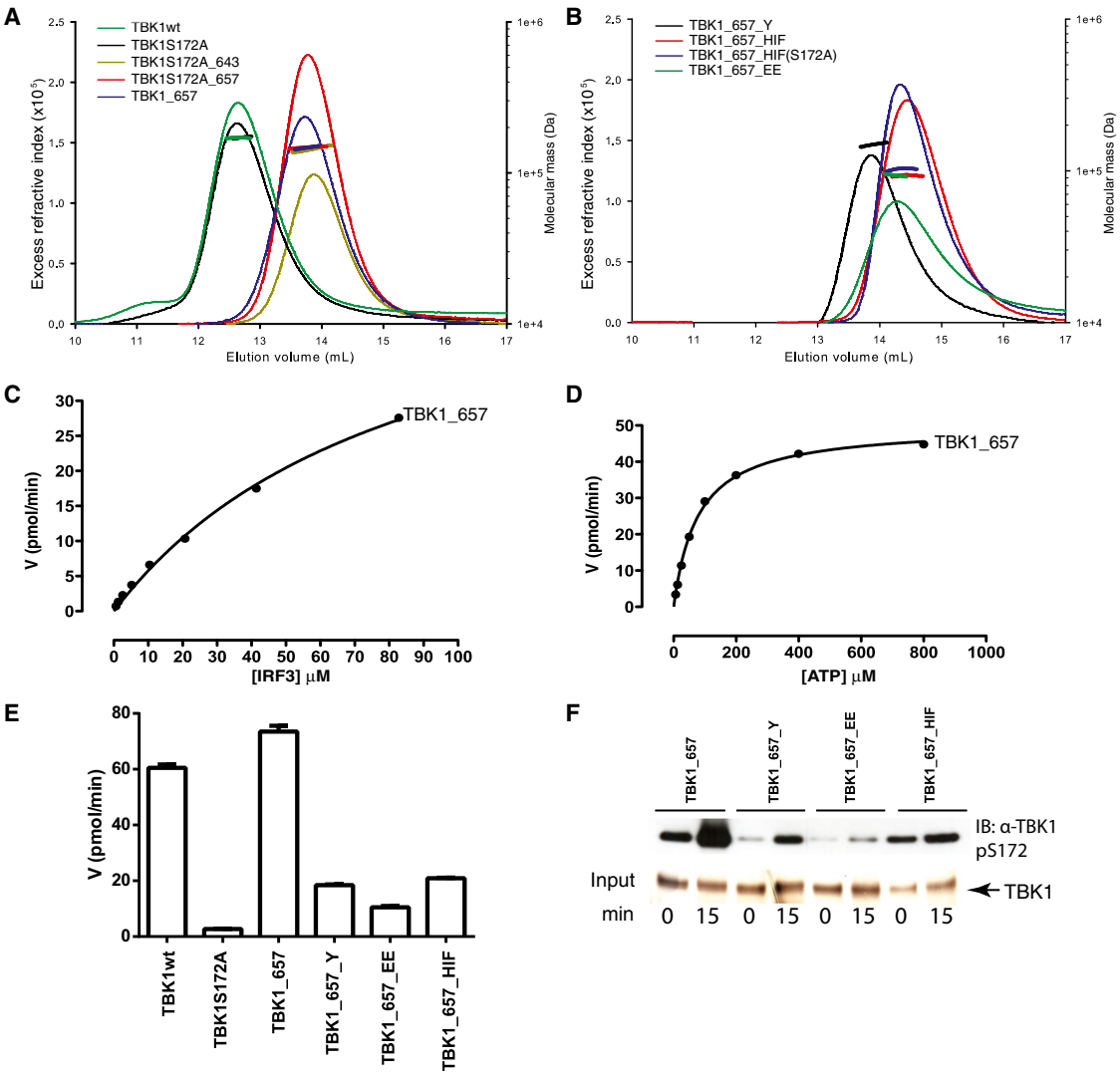

Figure 5. Analysis of Dimerization Mutants

(A) Size-exclusion chromatography and multiangle laser-light-scattering profiles of purified autophosphorylated TBK1wt and mutants.

(B) Mutations in the dimerization interface result in monomeric TBK1.

(C) Kinase assay on IRF3.

(D) Measurement of apparent K_m and V_{max} for ATP.

(E) Kinase assay using TBK1 mutants.

(F) TBK1 activation via S172 autophosphorylation. TBK1 mutants were analyzed by anti-pS172 immunoblotting after 0 or 15 min incubation as in (E). Silver-stained inputs are shown below.

See also Figure S1.

disruption of SDD- and ULD-mediated dimerization at interfaces III and IV interferes with TBK1 activation by reducing autophosphorylation.

Small Angle X-Ray-Scattering Experiments and Interaction with the Adaptor Nap1

We next investigated the positioning of the CTD in phosphorylated and nonphosphorylated TBK1. We purified full-length TBK1wt, a S172A mutant (TBK1S172A), as well as truncations lacking the C-terminal CTD domain. Mass spectroscopy showed that TBK1wt was phosphorylated on seven positions and that TBK1S172A was completely devoid of phosphorylation, confirming that phosphorylation of the activation loop is required for TBK1 autophosphorylation (Figures S1A and S1B). Among the seven autophosphorylation sites, five could be identified by phosphopeptide mapping of tryptic fragments on residues S499, S510, S518, T542, and S632 (data not shown). We did not observe a phosphopeptide comprising S172 in the T-loop of the kinase. However, previous data show that overexpression results in autophosphorylation of this residue and allows purification of active kinase (Kishore et al., 2002; Panne et al., 2007). Several of the phosphorylation sites observed here have

been previously reported in TBK1 kinase isolated from cells, and they are likely to be relevant for TBK1 regulation (Oppermann et al., 2009). We performed three experiments to investigate whether the TBK1 CTD folds back as originally proposed for IKKβ; however, none of the results supported the model. First, we probed the phosphorylated and nonphosphorylated conformations of TBK1 by limited proteolysis with trypsin. In nonphosphorylated TBK1S172A, the first cleavage event occurred C-terminal of K661, indicating that the CTD is flexibly attached to the kinase (Figure S1C). TBK1wt yielded a similar digestion pattern, suggesting no gross conformational changes upon autophosphorylation. Second, we performed SEC-MALLS experiments. Whereas major conformational rearrangements upon autophosphorylation of the dimer would likely have yielded altered hydrodynamic properties, the phosphorylated and nonphosphorylated forms gave identical profiles (Figure 5A). We used TBK1S172A truncated at K661 (TBK1S172A_661), as it was better behaved in solution, to perform analytical ultracentrifugation and also confirmed that it was a dimer (Figure S5). Third, we performed small angle X-ray scattering (SAXS) experiments to analyze the structure of the dimer in solution and to evaluate positioning of the CTD (Figure 6). We first measured scattering intensity patterns from two nonphosphorylated constructs, full-length TBK1S172A and TBK1S172A_661 (Table S2). The molecular envelope calculated from the SAXS data for TBK1S172A_661 showed excellent agreement with that calculated from the crystal structure (χ values of <3.2; Figure 6C). These envelopes fit neatly within that calculated from the SAXS data from full-length TBK1S172A, which contains residual volume at the C-terminal extremity of the SDD (Figure 6C). The scattering mass of this volume matches the expected size of the CTD, suggesting that the bulk of the CTD residues are located here (Rushe et al., 2008). These data suggest that, in inactive TBK1, the CTD does not fold back toward the KD but is fully extended. Also, these data show that, even in the absence of a stabilizing kinase inhibitor, the conformation of the TBK1 dimer in solution is in agreement with that seen in the crystal structures.

IKK kinase signaling requires interaction with scaffold proteins. Whereas NEMO scaffolds assembly of IKKα and IKKβ complexes, TBK1 interacts only indirectly with NEMO through the adaptor protein TANK (TRAF family member-associated NFκB activator) (Pomerantz and Baltimore, 1999; Zhao et al., 2007). In addition to TANK, three other adaptor proteins have been shown to directly interact with TBK1: NAP1 (NFκB activating kinase associated protein 1 or 5-azacytidine-induced protein 2 (Azi2)), SINTBAD (similar to NAP1 TBK1 adaptor) and optineurin, all of which share a TBK1/IKKε binding domain (TBD) predicted to form an α-helical structure (Fujita et al., 2003; Gatot et al., 2007; Goncalves et al., 2011; Guo and Cheng, 2007; Morton et al., 2008; Ryzhakov and Randow, 2007). All four adaptors are structurally similar to NEMO, suggesting a similar mode of action (Chau et al., 2008). Crystallographic studies show that NEMO forms a parallel coiled-coil homodimer and functions as a linear platform for assembly of the IKKα/β kinases (Israël, 2010). A N-terminal IKK binding domain of NEMO associates with the C-terminal NEMO binding domain (NBD) of IKKα/β kinase (Rushe et al., 2008). To further investigate scaffold binding and the role of TBK1 autophosphorylation in that process, we expressed and purified the His-tagged TBD domain of NAP1 (216–255) and performed pull-down assays with various TBK1 constructs. We found that the TBD of Nap1 interacted with full-length TBK1 irrespective of phosphorylation status (Figure 6D, lanes 5 and 7, and 9 and 11). Deletion of the C-terminal 67 residues of TBK1 abolished this interaction (Figure 6D, lanes 14 and 16), showing that NAP1 interacts in a constitutive manner directly with the C terminus of TBK1. To investigate if disruption of TBK1 dimerization affects adaptor binding in vivo, we cotransfected TBK1 dimerization mutants and NAP1 and performed coimmunoprecipitation experiments. We found that mutagenesis of dimerization interfaces did not interfere with Nap1 binding, suggesting that TBK1 dimerization is not required for adaptor binding (Figure 6E).

DISCUSSION

The TBK1 structures presented here show that the trimodular architecture with the KD, ULD, and SDD domains is conserved both among canonical and noncanonical IKKs. However, the relative domain orientations of KD, ULD, and SDD differ between the TBK1 and IKKβ kinase structures and as a result, the overall organization of the kinase dimers is different: whereas the TBK1 dimer is compact and stabilized through extensive dimerization interfaces, the IKKβ dimer is in a more "open" conformation. As IKKβ was crystallized using a construct that renders the kinase constitutively active, we considered that these structural differences reflect different activation statuses of IKK kinases and that reversible dimerization through interfaces I–III might be regulatory. However, none of our results supports this model: comparison of active and inactive TBK1 shows that activation reorganizes the KD into an active configuration while maintaining the compact dimer conformation. SAXS experiments also confirm that the structure of the compact dimer is maintained in solution even in the absence of inhibitor. We therefore rule out the possibility that dimer opening is part of a regulatory mechanism for TBK1.

In IKKβ, dimerization is mediated by a single SDD-SDD interface. The region of helix α4 s that is required for IKKβ/α homo- or heterodimerization is not essential for TBK1 dimerization. Instead, dimerization in the C-terminal part of the SDD (dimerization interface IV) is mediated by helix α1 s. These differences explain why noncanonical IKKs do not heterodimerize with canonical IKKs (Pomerantz and Baltimore, 1999). TBK1 is most closely related in sequence to IKKε, and it has been proposed that noncanonical IKKs also homo- and heterodimerize (Chau et al., 2008). However, we were unable to obtain evidence for a direct interaction between TBK1 and IKKε in immunoprecipitation experiments (data not shown). Analysis of sequence conservation shows that residues in the SDD dimerization interface are conserved only among TBK1 orthologs (Figure S3). TBK1 is constitutively expressed in a number of cell types, whereas IKKε expression is inducible by various cytokines (Shimada et al., 1999). The IFN-β gene is not activated in response to inducers in TBK1-deficient cells, but IFN production is unaffected in IKKε-deficient cells (Tenoever et al., 2007). Whereas TBK1-deficient cells show strong defects in IFN production in response to inducers, IFN production is induced normally in IKKε-deficient

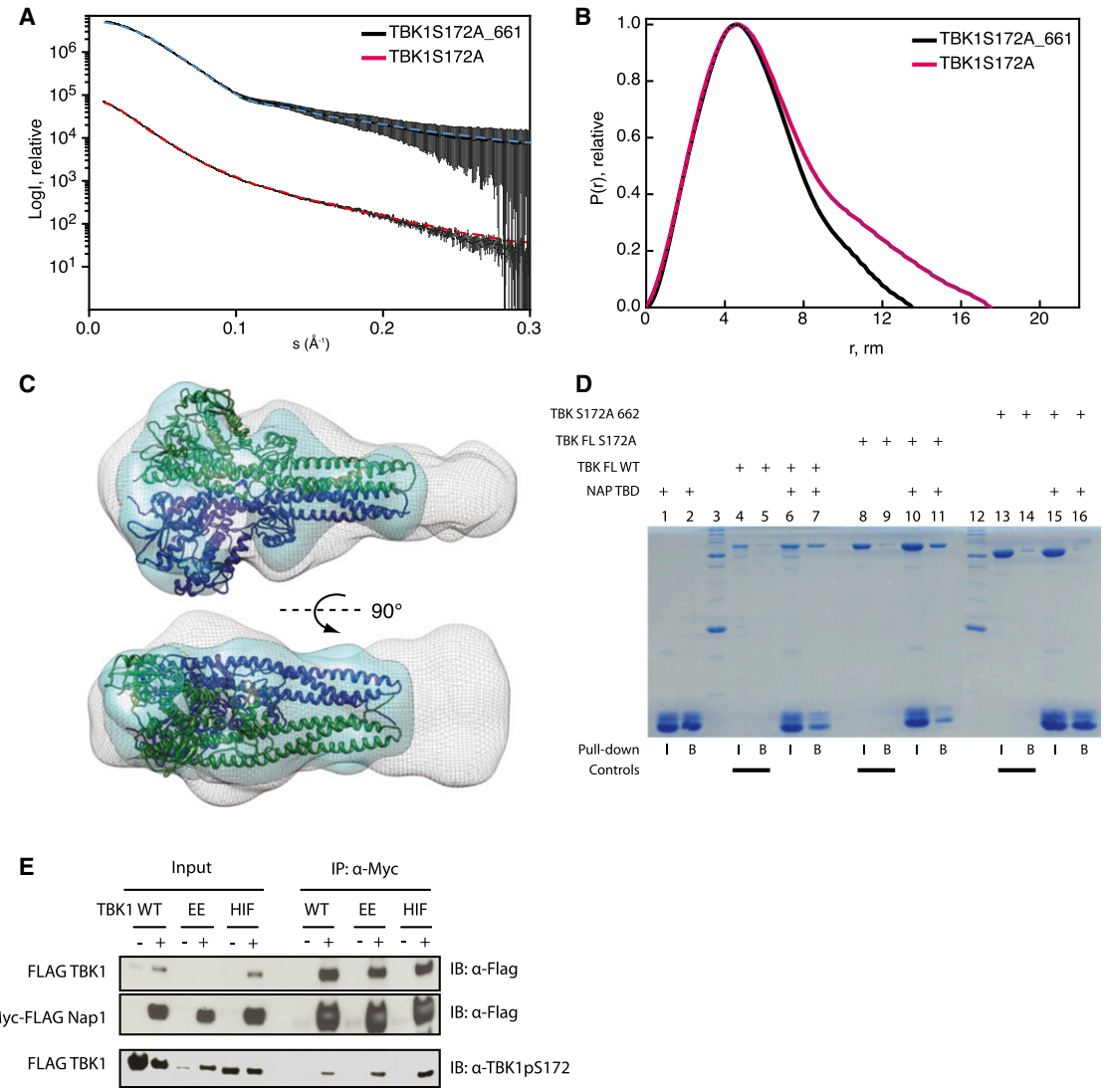

Figure 6. SAXS of TBK1 and Nap1 Interaction

(A) The experimental SAXS profile (log intensity [I] as a function of the momentum transfer [s]). Dots with error bars are the experimental scattering data. The superimposition of the best-fit ab initio model generated by DAMMIN is shown as a dashed line. TBK1S172A (black), TBK1S172A_661 (red). Calculated curves from the crystal structure as computed by CRYSOL (blue).

(B) Normalized interatomic distance distribution functions.

(C) Surface representation of the ab initio model of TBK1 kinase. The SAXS envelope of TBK1S172A is shown as a gray mesh and SAXS envelope of TBK1S172A_661 in light blue. The middle and bottom views are rotated counter clockwise by 90° around the horizontal axis.

(D) Interaction between TBK1 and Nap1 in vitro. Pull-down of TBK1 constructs using GST-NAP1 TBK1 binding domain (TBD) showing interaction between the NAP1 TBD and the CTD of TBK1.

(E) Interaction between TBK1 mutants and Nap1 in vivo. 293T cells were transfected with FLAG TBK1wt or mutants alone (−) or together with Myc-FLAG Nap1 (+). Left panel: input samples were loaded as a control. Right panel: coimmunoprecipitation (IP) experiments were performed using anti-Myc matrix beads and immunoblotted (IB) for anti-FLAG tagged or anti-pS172 protein.

See also Figure S5.

cells. However, IKKε-negative cells, unlike the TBK1 minus cells, display a defective IFN-inducible antiviral transcriptional response (Hemmi et al., 2004; Ng et al., 2011; Tenoever et al., 2007). Thus, TBK1 functions primarily in the virus-inducible expression of type I IFNs by phosphorylating IRF3 and IRF7, while IKKε functions in the downstream IFN induction pathway by phosphorylating STAT1 (Ng et al., 2011; Tenoever et al., 2007). It is interesting to note that both TBK1 and IKKε phosphorylate a specific set of serine residues in the C termini of IRF3 and 7, while IKKε, but not TBK1, specifically phosphorylates serine 708 in STAT1 (Tenoever et al., 2007). We propose that TBK1 does not heterodimerize with other IKKs, including IKKε, consistent with the nonoverlapping functions of the two kinases in vivo.

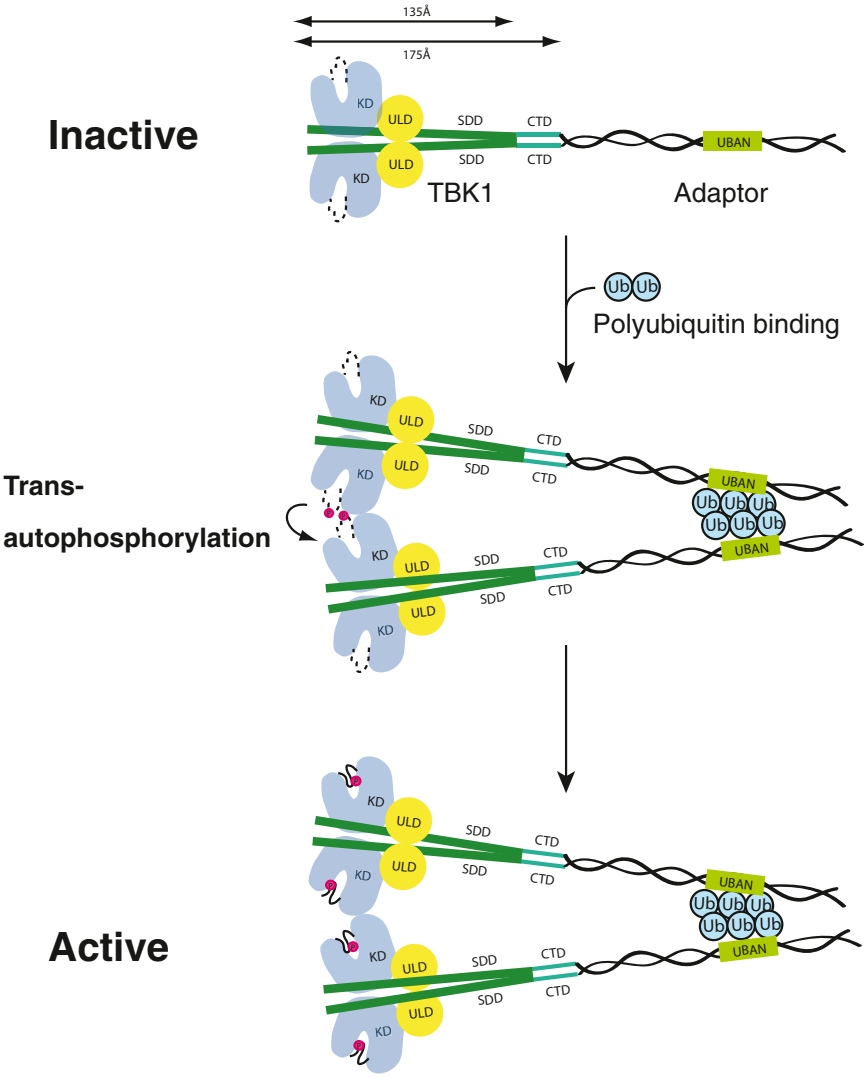

Figure 7. Model for TBK1 Activation
Adaptor proteins such as Nap1 or optineurin bind constitutively to the kinase CTD. Binding of K63-linked or linear polyubiquitin chains to the UBAN domain in the adaptor proteins triggers higher-order oligomerization of TBK1-adaptor complexes resulting in *trans*-autophosphorylation and activation of TBK1.

Noncanonical IKKs contain a single phosphoacceptor site (S172 in TBK1) in the activation loop of the KD, whereas canonical IKKs contain two such sites (S177/S181 in IKKβ). Whereas phosphomimetic mutations of the phosphoacceptor sites inactivate TBK1 or IKKε, such mutations in IKKα/β lead to constitutive activation (Kishore et al., 2002). Comparison of active, pS172-phosphorylated TBK1 with xIKKβ containing phosphomimetic residues E177 and E181 shows that these phosphoacceptor sites play different roles in noncanonical and canonical IKKs: in TBK1, pS172 makes several contacts with residues in the KD resulting in stabilization of the activation segment. This coordination cannot be achieved by phosphomimetic residues. In contrast, in the ordered activation segment of IKKβ, the E177 and E181 residues are mostly solvent exposed indicating the different roles of the phosphoacceptor sites in regulating noncanonical and canonical IKKs.

The geometry of TBK1, with the two KDs positioned on opposite faces of the dimer, precludes autophosphorylation and activation in *cis*. It is likely that activation requires *trans*-autophosphorylation through higher-order oligomerization of TBK1 dimers (Figure 7). In agreement with this model, mutants that interfere with TBK1 dimerization show significantly reduced *trans*-autophosphorylation. One possibility is that *trans*-autophosphorylation occurs through an activation loop swapped intermediate in which the S172 from one protomer is located in close proximity to the active site of a neighboring protomer (Ma et al., 2012). Once activated, monomeric KD or full-length TBK1 displays comparable kinase activities showing that higher-order oligomerization is not essential to maintain kinase activity after activation (Ma et al., 2012). Similarly, IKKβ dimerization is required for activation, but dimerization is not required for activity once the activation loop is phosphorylated (Xu et al., 2011). We therefore conclude that dimerization is required for TBK1 kinase activation but not for activity once the kinase is activated.

Adaptor proteins such as NEMO for IKKα/β and TANK, NAP1, SINTBAD, and optineurin for TBK1/IKKε form parallel coiled-coil homodimers that constitutively bind to the kinase CTD in a mutually exclusive manner (Figure 6C) (Goncalves et al., 2011). Disruption of TBK1 dimerization does not abolish interaction with Nap1 showing that kinase dimerization is not a prerequisite for adaptor binding. This is in agreement with the structure of the NEMO/IKK kinase associating domain in complex with segments of the IKKα/β, which shows that the NEMO dimer binds two IKK fragments independently (Rushe et al., 2008). However it is likely that adaptor binding stabilizes the C terminus of the kinase dimer and is important for TBK1 activation under physiological circumstances (Goncalves et al., 2011). Several adaptor proteins contain ubiquitin-binding domains that bind K63-linked or linear polyubiquitin chains, and ubiquitin binding appears to contribute to TBK1 activation (Gleason et al., 2011; Liu and Chen, 2011). One possibility is that binding of polyubiquitin chains triggers higher-order oligomerization of TBK1-adaptor complexes, resulting in *trans*-autophosphorylation and activation of the kinase (Figure 7). A similar mode of activation has been proposed for the TAK1 kinase complex (Xia et al., 2009). In addition, recent studies have shown that TBK1 is polyubiquitinated on the KD

by K63-linked chains, which allows recruitment of NEMO (Friedman et al., 2008; Wang et al., 2012). An important question is if and how direct ubiquitination or ubiquitin binding to the adaptor proteins triggers kinase oligomerization and activation.

EXPERIMENTAL PROCEDURES

Structure Determination, Refinement, and Analysis

The structure of inactive TBK1 was determined by single-wavelength anomalous dispersion (SAD) in space group $P3_221$ at 3.2 Å resolution, from a selenomethione-labeled crystal of TBK1. Heavy atom parameter refinement and SAD phase calculations were performed with SHARP using anomalous signal from 14 selenomethionine sites. The electron density map was improved with solvent flattening using SOLOMON. SAD phasing statistics from 32 to 4.0 Å resolution included a phasing power (anomalous) of 2.35 an R_{cullis} (anomalous) of 0.50 and a mean figure of merit of 0.449. A final model for TBK1 was produced by iterative rounds of manual model building in Coot and refinement using PHENIX. The Dundee PRODRG2 Server was used to generate topology and restraint files of the inhibitor compounds for refinement. The final model contains residues 1–657 and was refined to a 2.6 Å resolution with an R_{work} and an R_{free} of 24% and 27%, respectively. No electron density was observed for residues 166–174 and 187–198 in the activation loop and residues 483–491 in the SDD. The register of helix α2 s of the SDD was verified by an anomalous difference map obtained from a selenomethione-labeled L508M mutant. Refinement was carried out by applying secondary structure restraints in the initial rounds of refinement. Analysis of the refined structure by MolProbity showed that there are no residues in disallowed regions of the Ramachandran plot and no residues in disallowed regions. The MolProbity all atom clash score was 11.0, placing the structure in the 93rd percentile (with 100th best) of structures refined at 2.6 Å or lower resolution. The structure of active TBK1 was determined by molecular replacement in space group $P6_522$ at 4.0 Å resolution, using a KD-ULD fragment as the search model. After positioning of the KD-ULD fragment, additional density for the SDD was apparent in a $2F_0$-F_c map. The full KD-ULD-SDD chain was obtained by superposition of the full TBK1 chain onto the partial KD-ULD model. A model of the KD in the active conformation (4EUU) was used to build the activation loop (Ma et al., 2012). A final model for active TBK1 was produced by manual model building in Coot and refinement using PHENIX. For further details, please refer to Extended Experimental Procedures.

ACCESSION NUMBERS

The atomic coordinates have been deposited in the Protein Data Bank under ID codes 4IW0 (TBK1 active, ligand BX795), 4IWO (TBK1 inactive, ligand MRT67215), 4IWP (TBK1 inactive, ligand BX795), and 4IWQ (TBK1 inactive, ligand MRT67307).

SUPPLEMENTAL INFORMATION

Supplemental Information includes Extended Results, Extended Experimental Procedures, five figures, and two tables and can be found with this article online at http://dx.doi.org/10.1016/j.celrep.2013.01.034.

LICENSING INFORMATION

ACKNOWLEDGMENTS

We thank Xinping Lin of EMBL Heidelberg and Luca Signor of the Institut de Biologie Structurale Grenoble for mass spectrometry and Marc Jamin, UVHCI Grenoble for support with MALLS. We thank Aline Le Roy and Christine Ebel, from the IBS platform of the Partnership for Structural Biology and the Institut de Biologie Structurale in Grenoble (PSB/IBS), for the assistance and access to the instrument of Analytical Ultracentrifugation. We thank the EMBL Grenoble Crystallization Facility for screening of crystallization conditions. We thank Claude Cochet, CEA Grenoble for support with ATPase assays. We thank Joanne Hough and Ed McIver from MRC Technology, Centre for Therapeutics Discovery for synthesizing and providing MRT67215. We thank Natalia Shpiro, MRC Protein Phosphorylation Unit, University of Dundee, Scotland for synthesizing MRT67307 and Philip Cohen for providing this compound. We thank Carlo Petosa and Stephen C. Harrison for critical reading of the manuscript. This work was supported by a grant from the Finovi Foundation.

Received: May 25, 2012
Revised: October 29, 2012
Accepted: January 28, 2013
Published: February 28, 2013

REFERENCES

Adli, M., and Baldwin, A.S. (2006). IKK-i/IKKepsilon controls constitutive, cancer cell-associated NF-kappaB activity via regulation of Ser-536 p65/RelA phosphorylation. J. Biol. Chem. *281*, 26976–26984.

Baker, R., and Ghosh, S. (2009). Direct activation of protein kinases by ubiquitin. J. Mol. Cell Biol. *1*, 1–3.

Barbie, D.A., Tamayo, P., Boehm, J.S., Kim, S.Y., Moody, S.E., Dunn, I.F., Schinzel, A.C., Sandy, P., Meylan, E., Scholl, C., et al. (2009). Systematic RNA interference reveals that oncogenic KRAS-driven cancers require TBK1. Nature *462*, 108–112.

Boehm, J.S., Zhao, J.J., Yao, J., Kim, S.Y., Firestein, R., Dunn, I.F., Sjostrom, S.K., Garraway, L.A., Weremowicz, S., Richardson, A.L., et al. (2007). Integrative genomic approaches identify IKBKE as a breast cancer oncogene. Cell *129*, 1065–1079.

Chau, T.L., Gioia, R., Gatot, J.S., Patrascu, F., Carpentier, I., Chapelle, J.P., O'Neill, L., Beyaert, R., Piette, J., and Chariot, A. (2008). Are the IKKs and IKK-related kinases TBK1 and IKK-epsilon similarly activated? Trends Biochem. Sci. *33*, 171–180.

Chen, Z.J., Parent, L., and Maniatis, T. (1996). Site-specific phosphorylation of IkappaBalpha by a novel ubiquitination-dependent protein kinase activity. Cell *84*, 853–862.

Chien, Y., Kim, S., Bumeister, R., Loo, Y.M., Kwon, S.W., Johnson, C.L., Balakireva, M.G., Romeo, Y., Kopelovich, L., Gale, M., Jr., et al. (2006). RalB GTPase-mediated activation of the IkappaB family kinase TBK1 couples innate immune signaling to tumor cell survival. Cell *127*, 157–170.

Clark, K., Plater, L., Peggie, M., and Cohen, P. (2009). Use of the pharmacological inhibitor BX795 to study the regulation and physiological roles of TBK1 and IkappaB kinase epsilon: a distinct upstream kinase mediates Ser-172 phosphorylation and activation. J. Biol. Chem. *284*, 14136–14146.

Clark, K., Peggie, M., Plater, L., Sorcek, R.J., Young, E.R., Madwed, J.B., Hough, J., McIver, E.G., and Cohen, P. (2011). Novel cross-talk within the IKK family controls innate immunity. Biochem. J. *434*, 93–104.

Clément, J.F., Meloche, S., and Servant, M.J. (2008). The IKK-related kinases: from innate immunity to oncogenesis. Cell Res. *18*, 889–899.

De Bondt, H.L., Rosenblatt, J., Jancarik, J., Jones, H.D., Morgan, D.O., and Kim, S.H. (1993). Crystal structure of cyclin-dependent kinase 2. Nature *363*, 595–602.

DiDonato, J.A., Hayakawa, M., Rothwarf, D.M., Zandi, E., and Karin, M. (1997). A cytokine-responsive IkappaB kinase that activates the transcription factor NF-kappaB. Nature *388*, 548–554.

Fitzgerald, K.A., McWhirter, S.M., Faia, K.L., Rowe, D.C., Latz, E., Golenbock, D.T., Coyle, A.J., Liao, S.M., and Maniatis, T. (2003). IKKepsilon and TBK1 are essential components of the IRF3 signaling pathway. Nat. Immunol. *4*, 491–496.

Friedman, C.S., O'Donnell, M.A., Legarda-Addison, D., Ng, A., Cárdenas, W.B., Yount, J.S., Moran, T.M., Basler, C.F., Komuro, A., Horvath, C.M., et al. (2008). The tumour suppressor CYLD is a negative regulator of RIG-I-mediated antiviral response. EMBO Rep. *9*, 930–936.

Fujita, F., Taniguchi, Y., Kato, T., Narita, Y., Furuya, A., Ogawa, T., Sakurai, H., Joh, T., Itoh, M., Delhase, M., et al. (2003). Identification of NAP1, a regulatory subunit of IkappaB kinase-related kinases that potentiates NF-kappaB signaling. Mol. Cell. Biol. *23*, 7780–7793.

Gatot, J.S., Gioia, R., Chau, T.L., Patrascu, F., Warnier, M., Close, P., Chapelle, J.P., Muraille, E., Brown, K., Siebenlist, U., et al. (2007). Lipopolysaccharide-mediated interferon regulatory factor activation involves TBK1-IKKepsilon-dependent Lys(63)-linked polyubiquitination and phosphorylation of TANK/I-TRAF. J. Biol. Chem. *282*, 31131–31146.

Gleason, C.E., Ordureau, A., Gourlay, R., Arthur, J.S., and Cohen, P. (2011). Polyubiquitin binding to optineurin is required for optimal activation of TANK-binding kinase 1 and production of interferon β. J. Biol. Chem. *286*, 35663–35674.

Goncalves, A., Bürckstümmer, T., Dixit, E., Scheicher, R., Górna, M.W., Karayel, E., Sugar, C., Stukalov, A., Berg, T., Kralovics, R., et al. (2011). Functional dissection of the TBK1 molecular network. PLoS ONE *6*, e23971.

Guo, B., and Cheng, G. (2007). Modulation of the interferon antiviral response by the TBK1/IKKi adaptor protein TANK. J. Biol. Chem. *282*, 11817–11826.

Guo, J.P., Shu, S.K., He, L., Lee, Y.C., Kruk, P.A., Grenman, S., Nicosia, S.V., Mor, G., Schell, M.J., Coppola, D., and Cheng, J.Q. (2009). Deregulation of IKBKE is associated with tumor progression, poor prognosis, and cisplatin resistance in ovarian cancer. Am. J. Pathol. *175*, 324–333.

Hemmi, H., Takeuchi, O., Sato, S., Yamamoto, M., Kaisho, T., Sanjo, H., Kawai, T., Hoshino, K., Takeda, K., and Akira, S. (2004). The roles of two IkappaB kinase-related kinases in lipopolysaccharide and double stranded RNA signaling and viral infection. J. Exp. Med. *199*, 1641–1650.

Hicke, L., Schubert, H.L., and Hill, C.P. (2005). Ubiquitin-binding domains. Nat. Rev. Mol. Cell Biol. *6*, 610–621.

Ikeda, F., Hecker, C.M., Rozenknop, A., Nordmeier, R.D., Rogov, V., Hofmann, K., Akira, S., Dötsch, V., and Dikic, I. (2007). Involvement of the ubiquitin-like domain of TBK1/IKK-i kinases in regulation of IFN-inducible genes. EMBO J. *26*, 3451–3462.

Israël, A. (2010). The IKK complex, a central regulator of NF-kappaB activation. Cold Spring Harb. Perspect. Biol. *2*, a000158.

Karin, M., Yamamoto, Y., and Wang, Q.M. (2004). The IKK NF-kappa B system: a treasure trove for drug development. Nat. Rev. Drug Discov. *3*, 17–26.

Kishore, N., Huynh, Q.K., Mathialagan, S., Hall, T., Rouw, S., Creely, D., Lange, G., Caroll, J., Reitz, B., Donnelly, A., et al. (2002). IKK-i and TBK-1 are enzymatically distinct from the homologous enzyme IKK-2: comparative analysis of recombinant human IKK-i, TBK-1, and IKK-2. J. Biol. Chem. *277*, 13840–13847.

Kornev, A.P., and Taylor, S.S. (2010). Defining the conserved internal architecture of a protein kinase. Biochim. Biophys. Acta *1804*, 440–444.

Lei, M., Robinson, M.A., and Harrison, S.C. (2005). The active conformation of the PAK1 kinase domain. Structure *13*, 769–778.

Li, J., Li, J., Miyahira, A., Sun, J., Liu, Y., Cheng, G., and Liang, H. (2012). Crystal structure of the ubiquitin-like domain of human TBK1. Protein Cell *3*, 383–391.

Liu, S., and Chen, Z.J. (2011). Expanding role of ubiquitination in NF-κB signaling. Cell Res. *21*, 6–21.

Ma, X., Helgason, E., Phung, Q.T., Quan, C.L., Iyer, R.S., Lee, M.W., Bowman, K.K., Starovasnik, M.A., and Dueber, E.C. (2012). Molecular basis of Tank-binding kinase 1 activation by transautophosphorylation. Proc. Natl. Acad. Sci. USA *109*, 9378–9383.

Mercurio, F., Zhu, H., Murray, B.W., Shevchenko, A., Bennett, B.L., Li, J., Young, D.B., Barbosa, M., Mann, M., Manning, A., and Rao, A. (1997). IKK-1 and IKK-2: cytokine-activated IkappaB kinases essential for NF-kappaB activation. Science *278*, 860–866.

Morton, S., Hesson, L., Peggie, M., and Cohen, P. (2008). Enhanced binding of TBK1 by an optineurin mutant that causes a familial form of primary open angle glaucoma. FEBS Lett. *582*, 997–1002.

Möser, C.V., Kynast, K., Baatz, K., Russe, O.Q., Ferreirós, N., Costiuk, H., Lu, R., Schmidtko, A., Tegeder, I., Geisslinger, G., and Niederberger, E. (2011). The protein kinase IKKε is a potential target for the treatment of inflammatory hyperalgesia. J. Immunol. *187*, 2617–2625.

Ng, S.L., Friedman, B.A., Schmid, S., Gertz, J., Myers, R.M., Tenoever, B.R., and Maniatis, T. (2011). IκB kinase epsilon (IKK(epsilon)) regulates the balance between type I and type II interferon responses. Proc. Natl. Acad. Sci. USA *108*, 21170–21175.

Olefsky, J.M. (2009). IKKepsilon: a bridge between obesity and inflammation. Cell *138*, 834–836.

Oppermann, F.S., Gnad, F., Olsen, J.V., Hornberger, R., Greff, Z., Kéri, G., Mann, M., and Daub, H. (2009). Large-scale proteomics analysis of the human kinome. Mol. Cell. Proteomics *8*, 1751–1764.

Ou, Y.H., Torres, M., Ram, R., Formstecher, E., Roland, C., Cheng, T., Brekken, R., Wurz, R., Tasker, A., Polverino, T., et al. (2011). TBK1 directly engages Akt/PKB survival signaling to support oncogenic transformation. Mol. Cell *41*, 458–470.

Panne, D., McWhirter, S.M., Maniatis, T., and Harrison, S.C. (2007). Interferon regulatory factor 3 is regulated by a dual phosphorylation-dependent switch. J. Biol. Chem. *282*, 22816–22822.

Péant, B., Diallo, J.S., Dufour, F., Le Page, C., Delvoye, N., Saad, F., and Mes-Masson, A.M. (2009). Over-expression of IkappaB-kinase-epsilon (IKKepsilon/IKKi) induces secretion of inflammatory cytokines in prostate cancer cell lines. Prostate *69*, 706–718.

Peters, R.T., and Maniatis, T. (2001). A new family of IKK-related kinases may function as I kappa B kinase kinases. Biochim. Biophys. Acta *1471*, M57–M62.

Pomerantz, J.L., and Baltimore, D. (1999). NF-kappaB activation by a signaling complex containing TRAF2, TANK and TBK1, a novel IKK-related kinase. EMBO J. *18*, 6694–6704.

Rushe, M., Silvian, L., Bixler, S., Chen, L.L., Cheung, A., Bowes, S., Cuervo, H., Berkowitz, S., Zheng, T., Guckian, K., et al. (2008). Structure of a NEMO/IKK-associating domain reveals architecture of the interaction site. Structure *16*, 798–808.

Ryzhakov, G., and Randow, F. (2007). SINTBAD, a novel component of innate antiviral immunity, shares a TBK1-binding domain with NAP1 and TANK. EMBO J. *26*, 3180–3190.

Shimada, T., Kawai, T., Takeda, K., Matsumoto, M., Inoue, J., Tatsumi, Y., Kanamaru, A., and Akira, S. (1999). IKK-i, a novel lipopolysaccharide-inducible kinase that is related to IkappaB kinases. Int. Immunol. *11*, 1357–1362.

Steichen, J.M., Kuchinskas, M., Keshwani, M.M., Yang, J., Adams, J.A., and Taylor, S.S. (2012). Structural basis for the regulation of protein kinase A by activation loop phosphorylation. J. Biol. Chem. *287*, 14672–14680.

Tenoever, B.R., Ng, S.L., Chua, M.A., McWhirter, S.M., García-Sastre, A., and Maniatis, T. (2007). Multiple functions of the IKK-related kinase IKKepsilon in interferon-mediated antiviral immunity. Science *315*, 1274–1278.

Wang, L., Li, S., and Dorf, M.E. (2012). NEMO binds ubiquitinated TANK-binding kinase 1 (TBK1) to regulate innate immune responses to RNA viruses. PLoS ONE *7*, e43756.

Xia, Z.P., Sun, L., Chen, X., Pineda, G., Jiang, X., Adhikari, A., Zeng, W., and Chen, Z.J. (2009). Direct activation of protein kinases by unanchored polyubiquitin chains. Nature *461*, 114–119.

Xie, X., Zhang, D., Zhao, B., Lu, M.K., You, M., Condorelli, G., Wang, C.Y., and Guan, K.L. (2011). IkappaB kinase epsilon and TANK-binding kinase 1 activate AKT by direct phosphorylation. Proc. Natl. Acad. Sci. USA *108*, 6474–6479.

Xu, W., Harrison, S.C., and Eck, M.J. (1997). Three-dimensional structure of the tyrosine kinase c-Src. Nature *385*, 595–602.

Xu, G., Lo, Y.C., Li, Q., Napolitano, G., Wu, X., Jiang, X., Dreano, M., Karin, M., and Wu, H. (2011). Crystal structure of inhibitor of κB kinase β. Nature *472*, 325–330.

Zandi, E., Rothwarf, D.M., Delhase, M., Hayakawa, M., and Karin, M. (1997). The IkappaB kinase complex (IKK) contains two kinase subunits, IKKalpha and IKKbeta, necessary for IkappaB phosphorylation and NF-kappaB activation. Cell *91*, 243–252.

Zhao, T., Yang, L., Sun, Q., Arguello, M., Ballard, D.W., Hiscott, J., and Lin, R. (2007). The NEMO adaptor bridges the nuclear factor-kappaB and interferon regulatory factor signaling pathways. Nat. Immunol. *8*, 592–600.